Journal Pre-proofs

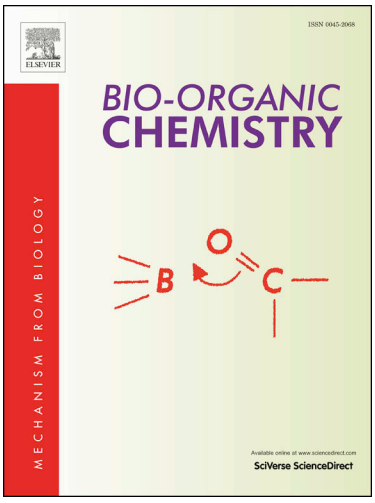

Anticancer properties, apoptosis and catecholase mimic activities of dinuclear cobalt(II) and copper(II) Schiff base complexes

M. Naqi Ahamad, Khushboo Iman, Md Kausar Raza, Manjeet kumar, Azaj Ansari, Musheer Ahmad, M. Shahid

PII: S0045-2068(19)31955-8
DOI: https://doi.org/10.1016/j.bioorg.2019.103561
Reference: YBIOO 103561

To appear in: *Bioorganic Chemistry*

Received Date: 16 November 2019
Revised Date: 15 December 2019
Accepted Date: 27 December 2019

Please cite this article as: M. Naqi Ahamad, K. Iman, M.K. Raza, M. kumar, A. Ansari, M. Ahmad, M. Shahid, Anticancer properties, apoptosis and catecholase mimic activities of dinuclear cobalt(II) and copper(II) Schiff base complexes, *Bioorganic Chemistry* (2019), doi: https://doi.org/10.1016/j.bioorg.2019.103561

Anticancer properties, apoptosis and catecholase mimic activities of dinuclear cobalt(II) and copper(II) Schiff base complexes

M. Naqi Ahamad[a], Khushboo Iman[a], Md Kausar Raza[c], Manjeet kumar[b], Azaj Ansari[b], Musheer Ahmad[d], M. Shahid[a*]

[a]*Department of Chemistry, Aligarh Muslim University, Aligarh-202002, India*
[b]*Department of Chemistry, Central University of Haryana, Mahendergarh-123031, Haryana, India*
[c]*Department of Inorganic and Physical Chemistry, Indian Institute of Science, Bangaluru, India*
[d]*Department of Applied Chemistry (ZHCET), Aligarh Muslim University, Aligarh-202002, India*
**E-mail: shahid81chem@gmail.com*

Abstract

The present work describes coordination chemistry and biological evaluation of two novel dinuclear complexes $[Co_2(HL^1)_2(H_2O)_2]\cdot 8H_2O$ (**1**) and $[Cu_2(L^2)_2]$ (**2**) obtained from the Schiff base ligands, H_3L^1 and H_2L^2 (formed *in situ*). The two complexes are characterized by single crystal X-ray, spectral and variable temperature magnetic and theoretical (DFT/TDDFT) analysis. X-ray analysis confirms both the complexes to be dinuclear with distorted octahedral and square pyramidal geometry around Co(II) and Cu(II) ions, respectively. Magnetic studies reveal presence of moderate antiferromagnetic interactions in both the complexes with J=98 (**1**) and 32 (**2**) cm^{-1}. The magnetic interactions are further cooroboratedby DFT studies. Co(II) complex (**1**) exhibited enhanced catecholase activity with K_{cat}= 213.48 h^{-1}, which is attributed to the greater extent of charge contribution on Co^{2+}as compared to Cu^{2+} as determined by DFT calculations. Furthermore, both the complexes show potent anticancer activity toward HeLa (cervical) and A549 (lung) cancer cell lineswith IC_{50} = 6-7 μM at 48 h, which ascertain both the complexes as better anticancer drugs than cisplatin. Furthermore, **1** and **2** exhibit apoptosis of Hela cells by demonstrating nuclear blebbingswith shrinking morphology. Hence, the present complexes could be employed as a model for metalloenzymes as well as potential anticancer substituents of cisplatin in future course.

Keywords: Schiff base complexes; anticancer activity; apoptosis; catecholase activity, DFT

1. Introduction

Chemistry of dinuclear metal complexes has been a promising research area which emphases on strong interaction of experimental and computational and theoretical studies.[1-4] From the very preparatory point of the chemistry of ligands and the metals, polymetallic complexes of Schiff bases are playing noteworthy role in the progress of coordination chemistry.[5] As evident from literature of such chemistry, the design, characterization and construction of binuclear transition metal complexes become important owing to the intriguing structures and fascinating applications in magnetism, optics, electronics, catalysis and fluorescence.[6-14] Combination of transition metals with multidentate Schiff base ligands which are mainly derived from o-vaniline or salicylaldehyde with aminoalcohols, provides a useful route for designing such complexes as these ligand systems facilitate terminal oxygen atoms to coordinate in bridging as well as chelating modes.[15-19] The Schiff base ligands containing flexible multidentate polyalcoholic groups facilitate the formation of clusters due to the presence of hydroxyl group which is a versatile O-donor.[20] Molecules with polyalcoholic groups are interesting moeities to construct functional chelating Schiff base ligands which with metal ions consequently yield different types of multinuclear complexes.[21] Polyalcoholic Schiff bases can coordinate to the metal either as neutral or mononegative terminal ligands forming a bridge between two or three metallic ions generating multinuclear complexes.[22,23] In this study, we report the design and synthesis of dinuclear Co^{II}-Co^{II} and Cu^{II}-Cu^{II} complexes by using two reduced Schiff base ligands with N,O,O,O or N,N,O,O donor sets alongwith a phenol group. Though some mono and polynuclear metal(II) complexes are reported to serve as active catalysts, reports on dinuclear systems as catecholase active agents are scarce.[24-26] Thereby we deduce that the catecholase activity can be tuned by various factors such as metal ion, metal ion combination, ligand environment, oxidation states of the metal ions and nuclearity of the complexes. Literature reveals that the catecholase activity revolves specifically around the complexes of

copper(II) ions and thus the assurance of the structure-action relationship has not been plausible.[27] Once again, regardless of the fact that a couple of dinuclear or oligonuclear mixes containing both Co^{III} and Co^{II} are known,[28,29] the likelihood of catecholase activity of dinuclear frameworks has not much been emphasised to the best of our knowledge.

Moreover, requirement of anticancer agents has increased during the last few decades due to increased cases of cancer.[30] There are many drugs available to treat cancer, however, with low selectivity[31] and much side effects.[32] These issues are needed to overcome and a proper drug with high efficacy and low side effects are a challenge now a days. Coordination chemistry has evoluted as a promising contributor towards cancer chemotherapy where different complexes with varying metal and ligand combination can tune the antiproliferative activity.[33] In this context combination of copper(II) metal ion with a Schiff base has been proven ultimate to exhibit anticancer properties. Specially, when the system is dinuclear, the effectiveness of the drug molecules has been observed to be much enhanced.[34] These factors led us design the two dinucear Schiff base systems screen for the anticancer activities towards the available HeLa and A549 cell line and the highest activity has been observed for Cu(II) complex toward both the cell lines even higher than cisplatin.

In the present study, two dinuclear complexes are designed and assessed for the catecholase activities and eventual catecholase activity has been examined only in dinuclear Co^{II} system.[35] The activity is either lesser, comparative or higher than those dinuclear cobalt systems reported in literature.[36-44] Our attempt was to synthesize dinuclear Co^{II} or Cu^{II} model complex with an oxygen donor rich ligand and to assess its catechol oxidase activity ans so we synthesized one cobalt and one copper complex with ligand H_3L^1 and H_2L^2 rich in O-donor sites, respectively. Different kinds of Schiff base ligands which form binuclear complexes are summarized in Scheme 1. The study of catecholase activity of **1** and **2** shows that only **1** which is Co^{II} dimer is active towards the catechol oxidation with K_{cat}=231.48 h^{-1}. The reaction is first order with

respect to substrate and follows the Michaelis-Menten kinetics. Moreover, the complexes are found to be potent toward the cervical (HeLa) and lung (A549) cancer cell lines to show apoptosis and these could be employed as anticancer drugs in future endeavors.

2. EXPERIMENTAL SECTION

2.1 Materials and method

$CoCl_2 \cdot 6H_2O$, $Cu(CH_3COO)_2 \cdot H_2O$, 2-amino-2-methyl-1,3-propanediol, o-vaniline, benzaldehyde, ethylenediamine, sodium hydroxide, triethylamine and methanol were purchased from the Sigma- Aldrich Chemical Co. India. All reagents of analytical grade were also purchased from commercial sources and used without further purification.

2.2 Physical methods

The FTIR spectra is recorded in the range 4000– 400 cm^{-1} from KBr pellets by using a Perkin Elmer Model range GX spectrophotometer. Melting points were controlled by the open capillary method and are uncorrected. The elemental C, H and N investigations has been performed from Micro-Analytical Laboratory of Central Medication Research Institute (CDRI), Lucknow, India. Perkin Elmer λ-45 UV visible spectrophotometer with cuvettes of 1 cm path length has been utilized to record the electronic spectra of 10^{-3} M solution in methanol.

2.3 X–ray crystal structure determination and refinements

Single crystal X-ray diffraction of **1** and **2** were performed at 296 K on a Bruker SMART APEX CCD diffractometer. X-ray data were collected using graphite monochromated Mo-*K*α radiation (λ= 0.71073 Å). The International Tables for X-ray Crystallography were used to determine the scattering factors for the atoms, the anomalous dispersion corrections and the linear absorption coefficients.[45] SAINT Software has been used to process the data integration and reduction.[46] An empirical absorption correction has been applied to the collected

reflections using SADABS[47] and the space group is determined using XPREP.[48] The structures were solved by direct methods using SIR-97[49] and refined on F^2 by full matrix least squares using the SHELXL-2016/6 program package.[50] Solvent masking of the highly disordered molecules was done using SQUEEZE command. The void electron count and void volume pertaining to which were squeezed. Anisotropic displacement parameters have been used to refine all non-hydrogen atoms. A summary of the crystallographic data and the structure refinement for the complexes has been mentioned in Table 1. Selected bond lengths and angles have been summarized in Tables S1 and S2 (ESI).

2.4. Synthesis

2.4.1. Synthesis of $[Co_2(HL^1)_2(H_2O)_2]\cdot 8H_2O$ (1)

1 has been synthesized using mechanism depicted in Scheme 2 where the ligands are formed first *in situ* and then complexation with metal salt occurs. The Schiff base ligand (H_3L^1) has been prepared by reacting o-vaniline (0.3 mmol, 0.045 g) and 2-amino-2-methyl-1,3-propanediol ($ampdH_2$) (0.3 mmol, 0.031 g) in mix solvent (15 mL methanol and 15 mL dichloromethane) at room temperature. The solution has been stirred for 12 h, and the resulting yellow color solution formed was treated with $CoCl_2$ (0.3 mmol, 0.071 g) which follows the addition of two drops of triethylamine. The color of solution turns wine red upon overnight stirring at room temperature. The resulting solution is filtered to obtain dark red block shaped crystals of **1** suitable for X-ray analysis within a period of one week. The solubility of synthesized complex has been found in methanol, ethanol, acetone, and water. The complex decomposes at 260 °C. Yield: 52%, Elemental Analysis (%): C = 37.31, H = 6.52,N = 3.63; Calc. for $C_{24}H_{50}Co_2N_2O_{18}$: C = 37.15, H = 6.04, N = 3.47. FTIR spectra (KBr pellets, cm^{-1}): ν(C=N), 1633 cm^{-1}; ν(C–H), 1444 cm^{-1}; ν(Co–O–Co), 1177 cm^{-1}; ν(Co–O), 743 cm^{-1}; ν(Co–N), 628 cm^{-1}.

2.4.2. Synthesis of $[Cu_2(L^2)_2]$ (2)

2 has also been synthesized according to the procedure adopted for **1** (Scheme 3). The Schiff base ligand (H_2L^2) are generated *in situ* by the combination of benzaldehyde and ethylenediamine in 2:1 molar ratio with mix solvent (15 ml methanol and 15 ml dichloromethane). The solution is then set to reflux with continuous stirring for 3 h at 60 °C and is allowed to stand for cooling at room temperature. This cooling is followed by the dropwise addition of $Cu(OAc)_2 \cdot H_2O$ (1 mmol, 0.199 g) and then 1 mmol NaOH to the Schiff base ligand (H_2L^2) that turns the solution into green. The solution is stirred overnight at ambient temperature. The resulting solution is filtered. Dark blue block shaped crystals of **2** suitable for X-ray analysis have been obtained within a period of two weeks. The solubility of synthesized complex has been found in acetonitrile, acetone and water. The complex decomposes at 240 °C. Yield: 48%. Elemental Analysis (%): C = 58.29, H = 4.21,N = 8.43; Calc. for $C_{32}H_{28}Cu_2N_4O_4$: C = 58.26, H = 4.28,N = 8.49. FTIR spectra (KBr pellets, cm^{-1}): ν(C=N), 1630 cm^{-1}; ν(C–H), 1449 cm^{-1}; ν(Cu–O–Cu),853 cm^{-1}; ν(Cu–O), 734 cm^{-1}; ν(Cu–N), 572 cm^{-1}.

2.5. Catecholase activity

To a solution of 10^{-4} M of **1** in methanol, 100 equivalents of 3,5-di-tert-butylcatechol (3,5-DTBC) in methanol have been added under aerobic condition at room temperature. Spectrophotometric data have been reported by generating absorbance versus wavelength (wavelength scan) plots at a regular time intervals of 10 min in the range 200−700 nm. 10^{-4} M solution of the complex has been treated with 10, 30, 50, 70, and 100 equivalents of a substrate to determine the substrate concentration dependence of the rate and to determine various kinetic parameters. The reactions are followed spectrophotometrically by monitoring the increase in

absorbance at 401 nm (corresponding to the quinone band maxima) as a function of time (time scan).

2.6. Anticancer activity

2.6.1.Cytotoxic assay

HeLa cells have been picked from maintenance cultures in the logarithmic phase, after counting in a hemocytometer using a trypan blue solution. The cell concentration is adjusted to 5×10^4 cells ml^{-1} and the cells are plated in 96 well flat bottom culture plates and incubated for 24 or 48 h with various concentrations of the test compounds. MTT dye reduction assay is used to determine the effect of the drugs on cancer cell viability by measuring the optical density at 590 nm using a micro-plate reader spectrophotometer (Perkin- Elmer 2030).[51]

2.6.2. Nuclear staining

Nuclear staining using the DAPI stain has been performed according to the method previously described.[52] Concisely, HeLa cells either treated or untreated with test compounds are smeared on a clean glass slide, cells have been fixed with 3.7% formaldehyde for 15 minutes, permeabilized with 0.1% Triton X-100 and stained with 1 μg mL^{-1} DAPI for 5 min at 37 °C. The cells are then washed with PBS and examined by fluorescence microscopy (Olympus IX 71) to confirm any condensation or fragmentation of the nuclei indicating cells undergoing apoptosis.

2.7. Computational details

Gaussian09 program package has been used to perform all the DFT computations.[53] B3LYP–D2 functional have been employed for the optimizations of structures.[54-56] This functional is reknowned for the predictions of correct spin state structures and energies of molecular complexes.[57] The LanL2DZ[58-61] and 6–31G[62] basis sets have been used for the Co/Cu centers

and other organic elements (C, H, O and N), respectively. Single point energy calculations are also performed to compute through Polarized Continuum Model (PCM)[63] using TZVP[64-65] basis set where methanol is used as solvent. All positive values of vibrational frequencies of optimized geometries are ensured the local minima. The time dependent density functional theory (TD–DFT) calculations have also been done for understanding the insight of electronic transitions with the help of ORCA 4.0.1 software.[66] The calculations of charge distribution among molecular orbitals of the Co/Cu complexes have been performed by Chemmisian software[67]. Hydrogen atoms are omitted for the clarity of the presented structures.

3. Results and discussion

3.1. Synthesis

Both the Schiff base ligands have been synthesized *in-situ*. H_3L^1 is synthesized by the reaction of 2-amino-2-methyl-1,3-propanediol and o-vaniline in methanol and dichloromethane medium (Scheme 2) while H_2L^2 has been derived by the mixture of ethylenediamine and benzaldehyde also in mixed solvent (methanol and dichloromethane) (Scheme 3). Both the *in situ* formed Schiff base ligands (H_3L^1 and H_2L^2) upon treatment with cobalt chloride and copper acetate yielded **1** and **2**, respectively.

3.2. Single crystal X-ray studies

3.2.1. Structural Description of $[Co_2(HL^1)_2(H_2O)_2]\cdot 8H_2O$ (1)

1 crystallizes in the monoclinic system with space group $P2_1/c$ (Fig. 1 and Table 1) containing two cobalt centers. Selected bond angles and bond angles have been mentioned in Table S1 and S2. These two cobalt ions are present in octahedral environment having different arrangement of ligands. A partially labelled plot of the complex shows the dinuclear cation is resulted through two bridging alkoxo oxygen from Schiff base (H_3L^1) ligands. Both the cobalt

ions are present in +2 oxidation state as confirmed by the crystal structure and the bond valence summation (BVS) calculations (Table S3). One Co1 center is ligated by two Schiff base nitrogen (N1 and N2) coordinating trans to each other, and other four coordination sites, which are in plane and ligated by four oxygens. Out of four oxygens, the two oxygens form bridges between the Co1 and Co2 centers and rest of two oxygens belong to phenolic group of Schiff base ligand. Co2 center has two oxygens of water molecule coordinating cis to each other on terminal position, two of four oxygens are bridged with Co1 center and rest of two oxygens of alcohols from Schiff base (H_3L^1) are coordinating trans to each other. The bond angles Co2–O4–Co1 and Co2–O8–Co1, are 95.68˚ and 98.60˚, respectively. The bond lengths, Co1–O4 (1.915 Å) and Co1–O8 (1.888 Å) are shorter than the Co2–O4 and Co2–O8 having values 2.078 Å and 2.018 Å, respectively. Due to these variations of angle and bond length, both cobalt centers are showing slightly distorted octahedral geometry. The Schiff base ligand behaves as a tetradentate negative O_3N-donor ligand with both chelating and bridging modes when coordinate to the cobalt centers. Each Schiff base (H_3L^1) ligand adopts two five membered rings and two six membered ring. The crystal structure of **1** is stabilized by non-covalent O–H□□□O, C–H□□□O and O–H□□□Co interactions. Formation of a 1 D polymeric chain has been observed due to the presence of strong O–H□□□O and C–H□□□O hydrogen bonding interactions as shown in Fig. 2. Each cluster forms ten hydrogen bonds with neighboring moieties, resulting in "Zig-Zag" 1 D polymer chain. In crystal lattice, there are four water molecules, which also consolidate the structures.

3.2.2. Crystal structure of $[Cu_2(L)_2]$ (2)

The molecular structure of **2** is illustrated in Fig. 3. Selected bond lengths and bond angles have been given in Tables S1 and S2. **2** crystallizes in monoclinic system with C 2/c space group (Table 1) containing two copper centres. Two Cu(II) ions and two dianionic Schiff bases result in the formation of neutral dimeric $Cu_2(L^2)_2$ moiety. Both the Cu(II) ions in the **2** adopt penta-

coordinate environment having square pyramidal geometry. The oxidation state of both each copper ion is +2 which is ascertained by the crystal structure and the bond valence summation (BVS) calculations (Table S3). Each Schiff base has two nitrogen atoms (N1 and N2) and two oxygen atoms (O1 and O2) coordinated to Cu(II) ion in square pyramidal manner. Both Cu(II) centers are linked via μ_2-bridged provided by oxygen (O1) of each Schiff base ligand (H_2L^2). The Schiff base acts as tetradentate dinegative (O_2N_2) donor ligand, which adopts both chelating and bridging modes when coordinate to the Cu(II) centers. Each Cu(II) center forms two six-membered and one five-membered ring. Asymmetric unit of **2** contains one Cu(II) ion having square planar geometry. Each Cu(II) ion possesses three phenoxide oxygen atoms in which two oxygens are μ_2-bridged and one oxygen is on terminal position. Axial bond length of both Cu(II) ions is longer than equatorial bond length. Due to axial bond elongation, **2** has slightly distorted square pyramidal geometry. The structure of **2** is stabilized by C–H□□□O, C–H□□□M and C–H□□□C interactions. There are two types of polymeric chains i.e. 1 D and 2 D. Both intermolecular as well as intramolecular H-bonding has been noticed in the crystal lattice. 1 D polymer chain is generated as a result of intermolecular H-bonding while 2 D polymeric sheet is generated due to the occurance of both intra and intermolecular H-bonding (Fig. 4).

3.3 FTIR, UV-visible and PXRD

The presence of imine, metal nitrogen bonding, metal oxygen bonding of water and alcohols and aryl-alkyl ether of Schiff base ligand have been characterized by FTIR spectra of **1** and **2** that give rise to a number of characteristic vibrations (Fig. S1, ESI). The spectra give sufficient information about the nature of Schiff base ligand and their coordination modes with different metal ions. The spectrum of **1** shows a broad peak in the range of 3400-3200 cm^{-1} which can be assigned to the free water molecule in the moiety.[68] Both **1** and **2** show strong peaks due to imine characteristic (C=N) function at 1633 and 1630 cm^{-1}, respectively. Only **1** having phenyl-

methyl ether group on the Schiff base ligand exhibits a characteristic band at 1249 cm^{-1}. Bending vibrations of methylene and methyl groups, v(C-H) appear in the range 1470-1444 cm^{-1}. Further, the bridging M–O–M bonding gives a peak at 1177 and 853 cm^{-1} in **1** and **2**, respectively. Bands due to M–Oand M–N bonds appear in the region 400-450 cm^{-1}. The electronic spectra of the aqueous solutions (10^{-3} M) of the complexes exhibit number of bands corresponding to ligand-to-metal charge transfer (LMCT) and $\pi \rightarrow \pi^*$ transitions besides those attributed to the ligand field (d-d) transitions arising from the crystal field splitting (Fig. S2, ESI). **1** and **2** show highest energy vibrational bands at 256, 365, 390 and 220, 240, 255 nm, respectively, assignable to charge transfer (L→M).[69] The relatively weak intensity broad bands at 525, 700 nm (**1**) or 558 nm (**2**), characteristic of ligand field d-d transitions of the metal ions have been observed in visible region of the spectra. The phase purity of the complexes was ascertained by powder X-ray diffraction (PXRD) analysis. The as-synthesized and simulated PXRD patterns were identical confirming the bulk purity of **1** and **2** (Fig. S3, ESI).

3.4. Magnetic studies

A dinuclear core is formed as a result of bridging of two metal centers via two doubly bridged alkoxides. **Fig. 5** illustrates that there are two types of Co–O(R)–Co bond angles (95.68 and 98.60°). The $\chi_M T$ product at 300 K has been found to be 5.7 cm^3 K mol^{-1} for **1** which is higher than the spin-only value of 3.75 $cm^3 K mol^{-1}$ for two non-interacting co(II) centers ($S = 3/2$, $g = 2$ leads to C = 15/8 cm^3 mol^{-1} per Co^{II} ion) (**Fig. 5**). We evaluate C = 2.84 cm^3 mol^{-1} per ion leading to $g = 2.44$ from this $\chi_M T$ product at room temperature. Similar trends have been found in common for clusters containing Co^{II} ions and shows the influence of the unquenched orbital angular momentum on the magnetic properties. $\chi_M T$ is found to be constant on decreasing the temperature upto 50 K. Further decrease in temperature led to the increament of $\chi_M T$ product that reaches to a maximum value of 6.0 cm^3 K mol^{-1} around 20 K. At lowest

measured temperatures the $\chi_M T$ product is decreased again. The moderate ferromagnetic interactions alongwith magnetic anisotropy are responsible for such trend of the $\chi_M T$ product. However, highly anisotropic systems like Co^{II} contradict such conclusions. The *M vs H* plots of **1,** at low fields, increases rapidly while much slowly at higher fields. However, no saturation has been observed until 7 T that supports the presence of magnetic anisotropy in the system. The magnetization value at the highest measured field (7 T) and the lowest temperature (2 K) is found to be 4.21 μ_B.

Free cobalt ions are seven times degenerate in the orbital angular momentum that pertains to the ^4F ground state. It tends to split into the three levels $^3A_2$, $^4T_2$ and $^4T_1$, with the latter being lowest in an octahedral ligand field. These levels are separated well by an energy difference in the order of ten thousand Kelvin. Thus, only the lowest level $^4T_1$ has to be regarded.

$$\hat{\mathbf{L}} = (-3/2)k\hat{\mathbf{l}}$$

Where, *k* being lesser than one.

The state $^4T_1$ consists of three orbital angular momentum states and can, therefore, be modeled by an effective orbital angular momentum l = 1, whose orbital angular momentum operator is related to the orbital angular momentum operator $\hat{L}$ in T_1 and P bases ($\hat{L}(T_1)=(3/2)\hat{L}(P)$.

Since $^4T_1$ has the same symmetry as the higher state ^4P, the symmetry mixing is from a $^4T_1$ term of ^4P states. This can be represented by introducing an orbital reduction factor k, yielding an orbital angular momentum operator.

Further splitting of $^4T_1$ ground state has been observed under the distortion of the ligand field and the spin-orbit coupling, yielding a sequence of Kramer's doublets with splitting on the order of several 100 K. The ground state Kramer's doublet is found to be thermally populated below temperatures of about 50 K only. Hence, the magnetic behaviour can be described by an

effective spin Hamiltonian with an effective spin τ = 1/2 for each Co^{II} center.[70,71] The advantage of this model is the dramatic reduction of the dimension of the Hilbert space. In this effective description, the magnetic couplings and g factors are anisotropic. Assumption of uniaxial anisotropy has been made to reduce the number of magnetic parameters. All *M vs. H* (Fig. 5, inset) and the χT curve at temperatures below 50 K have been fitted simultaneously to the following Hamiltonian to avoid over parameterization:

$$\hat{H} = -\left(J + \Delta J\right)\left(\hat{\tau}_{1,\mathrm{x}}\hat{\tau}_{2,\mathrm{x}} + \hat{\tau}_{1,\mathrm{y}}\hat{\tau}_{2,\mathrm{y}}\right) - J\hat{\tau}_{1,\mathrm{z}}\hat{\tau}_{2,\mathrm{z}} + \mu_{\mathrm{B}}\sum_{i=\{1,2\}}\left(g_{i,\mathrm{xy}}\left(\hat{\tau}_{i,\mathrm{x}}B_{\mathrm{x}} + \hat{\tau}_{i,\mathrm{y}}B_{\mathrm{y}}\right) + g_{i,\mathrm{z}}\hat{\tau}_{i,\mathrm{z}}B_{\mathrm{z}}\right) \quad (1)$$

Here, J is the coupling constant and ΔJ is the energy gaps between the ground and excited eigenvalues. The magnetic data of **1** are fitted and the magnetic parameters obtained are, J = 98(5) K, ΔJ = -49.0 (1.3) K, g_{xy} = 2.967(21), and g_z = 7.001(6). The data are indicative of the moderate ferromagnetic interactions between Co(II) centers.

The temperature dependence of the magnetic susceptibility for **2** has also been measured under an applied dc field of 0.1 T in the temperature range 2–300 K. Plot of χ_MT versus T (χ_M is the molar magnetic susceptibility per two Cu(II) ions) shows moderate ferromagnetic behavior for **2** (Fig. 6). The experimental χ_MT value at room temperature (1.01 cm^3Kmol^{-1}) is higher than the theoretical one expected for the two isolated copper(II) ions [$\chi_M T = 2(N\beta^2g^2/3k)S(S+1)$ = 0.749 cm^3 K mol^{-1}, wherein g = 2.00 is the spectroscopic splitting factor, *N* = Avogadro's number, β = the Bohr magneton, *k* = Boltzman's constant, and $S = ½$].[72] The plot exhibits the behavior of a weak ferromagnetically coupled dinuclear molecule with a continuous increase of the χ_MT value on lowering the temperature. This attains a maximum value of χ_MT i.e, 1.18 cm^3Kmol^{-1} at 28 K after which it starts to decrease slightly upto the χ_MT value of 1.12 cm^3Kmol^{-1} at 2 K. The *M vs H* curves of **1** increased rapidly at low fields in linear fashion and more slowly at higher fields (Fig. 6, inset). However, no saturation was observed until 7 T at 3

K. At 2 or 3 K, the magnetization value gets nearly saturated. The magnetization value at the highest measured field (7 T) and the lowest temperature (2 K) was 2.20 μ_B.

The magnetic behaviour has been modeled using a Heisenberg spin Hamiltonian for a dinuclear model (Eqn 2) and a fit of χ_MT vs. T to the Bleaney–Bowers expression (S = ½) (Eqn 3) using g = 2.20

$$\hat{H} = -2J\,[\hat{S}_1\hat{S}_2] \quad (2)$$

$$\chi_m(T) = \frac{2N\beta^2g^2}{K_BT}\,\frac{1}{3 + exp\left(-J/K_BT\right)} \quad (3)$$

Best-fit parameters were obtained by minimization of the agreement factor R (Eqn 4):

$$R = \frac{\Sigma(\chi_M^{calc}T - \chi_M^{exp}T)^2}{\Sigma(\chi_M^{exp}T)^2} \quad (4)$$

The temperature independent paramagnetic (TIP) contribution [49] is at first added in the calculation. The fitting gives J = 32(2) cm^{-1} with R =1.23 x 10^{-4} (g = 2.0 is adopted for fittings) showing presence of moderate ferromagnetic interactions between the two Cu(II) nuclei. The magnetic interactions in both the complexes have further been cooroborated by theoretical (DFT) studies (vide infra).

3.5 Catecholase activity

Dinuclear complexes derived from Schiff base ligands have been proven to show an efficent catecholase activity towards 3,5-di-tert-butylcatechol (3,5-DTBC). 3,5-DTBC has low quinone-catecholase reduction potential due to the presence of bulky tertiarybutyl substituents on its ring and tends to get easily oxidized to the corresponding quinone. The course of the reaction is followed by UV-Vis spectroscopy. The time dependent UV-Vis spectral scan is performed in pure methanol. 3,5-DTBC shows maximum absorption at 401 nm in methanolic

solution. Before implimenting the kinetics of the reaction in detail, we first need to check whether the dinuclear complex can oxidize the 3,5-DTBC. As a result of which 1×10^{-4} mol $dm^{-3}$of **1** and **2** under aerobic condition have been treated with the methanolic solution of 3,5-DTBC. After the addition of 3,5-DTBC to the methanolic solution of **1** and **2**, the reaction is examined for 2 hours. Upon addition of 3,5-DTBC the spectral run done immediately exhibits increment of the absorbance nearly above that band (Fig. 7) in case of **1**. **2** does not exhibit any noticeable change in spectral pattern after addition of 3,5-DTBC thus indicating its catechol oxidase inactivity. Kinetic study of the oxidation of 3,5-DTBC to 3,5-DTBQ facilitated by **1** is carried out by the method of initial rates, following the absorption increase at 401 nm. The experiment is performed with the complex (at constant concentration of 1×10^{-4} mol dm^{-3}) and 3,5-DTBC (varying the concentration from 1×10^{-3}mol dm^{-3} to 1×10^{-2} mol dm^{-3}) in methanol using a UV-Vis spectrophotometer. The experimental procedure includes the preparation of the substrate 3,5-DTBC and the stock solutions of the complex at higher concentration in pure methanol medium. Moreover, 2 ml of 3,5-DTBC at a proper concentration obtained by perfect dilution from the stock arrangement was taken into a UV-Vis quartz cell and kept for some time inside the cell holder, which was associated to a thermostat to keep the temperature 25 °C. Furthermore, 0.04 ml of the stock solution of the complex was added to it to accomplish a definitive concentration of the complex as 10^{-4} mol dm^{-3}. The formation of 3,5-DTBQ was examined with time. Applying the initial rate method to determine the value of the rate constant for each concentration of the substrate and each experiment was repeated three times. For the complex, the average rate constant value shows that the rate is first order at low concentration of the 3,5-DTBC substrate but zero order at high concentration of substrate. Figure 8 indicates the dependency of initial rates on substrate concentration for the oxidation of 3,5-DTBC to 3,5-DTBQ catalyzed by **1** in methanol. The rate dependency on the concentration of the substrate may be examined by the saturation kinetics and a treatment based on the Michaelis–Menten

model seemed to be appropriate. We consider the mechanism of formation of the catalyst-substrate complex (CS), which subsequently breaks down in the second step to form the free catalyst (C) and the product (P) as shown below:

$$C + S \underset{k_2}{\overset{k_1}{\rightleftharpoons}} CS \underset{k_4}{\overset{k_3}{\rightleftharpoons}} C + P$$

The above equation prompts to the well-known Michaelis–Menten equation:

$$V = \frac{V_{max}\ [S]}{K_M + [S]}$$

Where [S] = concentration of the substrate (3,5-DTBC); V = initial rate; $K_M = (k_2 + k_3)/k_1$, Michaelis–Menten constant for the metal complex and V_{max} = maximum initial rate attained for a specific concentration of the metal complex in the presence of a large excess of the 3,5-DTBC. The Michaelis–Menten equation can be changed algebraically into other arrangements that are more useful in calculating and plotting the data. Mostly used transformations is derived simply by taking the reciprocal of both sides of Michaelis-Menten equation which reduces to the well known Lineweaver– Burk Equation as follows:[73,74]

$$\frac{1}{V} = \frac{K_M}{V_{max}} \times \frac{1}{[S]} + \frac{1}{V_{max}}$$

The binding constant (K_M), maximum velocity (V_{max}), and rate constant for dissociation of substrates (i.e., turnover number, K_{cat}) were calculated for **1** using the Lineweaver–Burk graph of 1/V vs. 1/[S] (Fig. 6), using the above equation and the kinetic parameters are presented in Table 2. From the data, it is evident that the catecholase activity of the present complex is either lesser, comparative or higher than those similar dinuclear systems[36-38] obtained from the Schiff base ligands (Scheme 1).

3.6. Anticancer activity

3.6.1.Inhibition of cancer cell viability

We study the viability of A549 and HeLa cells using the MTT assay to assess the antiproliferative efficacy of **1** and **2**. A highly proliferative human cancer model is supported by A549 and HeLa cells. The complexes show a reduction in the viability of both A549 and HeLa cells in a dose-dependent manner. **1** and **2** gave the IC_{50} values in the range 7-30 and 6-19 μM for A549 and HeLa cell lines, respectively. At 24 h, A549 cell shows maximum IC_{50} value, i.e., 30.88 μM (**1**) and 17.74 μM (**2**), whereas at 48 h, these cell lines shows IC_{50} = 20.29 and 14.25 μM respectively, by **1** and **2**. Similarly, in HeLa cell, **1** and **2** shows the maximum value of IC_{50}, i.e., 30.20 and 19.89 μM at 24 h, whereas 7.339 and 6.722 μM at 48 h, respectively. Cytotoxic activity of **2** is found to be higher than **1** in both A549 and HeLa cells, which is directed by the IC_{50} values with the dose dependence listed in Table 3 and Fig 9. Overall impression supports that **1** and **2** show highest anticancer activity against HeLa cell lines at 48 h (with lowest IC_{50} values). These activities are even higher than those shown by well known drug cisplatin.

A conceivable single shot medication to check cancer growth has been unambigious until this point, because of their various events over a hundred structures, and a few instances of a repeat of disease post chemotherapy and medical procedure are outstanding. Interestingly, equating the efficacy of our synthesized novel copper and cobalt compounds against the presently available common chemo drugs sold to patients, we found that Cisplatin, Gefitinib, Gemcitabine, 5-Fluorouracil, and Vinorelbine had an IC_{50} of 13 μM, 20 μM, 35 μM, 40 μM and 48 μM, respectively, on HeLa cells under conditions similar to our experiment.[75] These findings would be proven to introduce our compounds (**1** and **2**) as future drug candidates with improved efficacy.

3.6.2. Nuclear staining assay

DAPI staining has been performed to investigate the apoptotic potential of test compounds (**1** and **2**) in HeLa cells. Chromatin condensation during the process of apoptosis (type I programmed cell death) is a characterizing marker of nuclear alteration. HeLa cells are treated with 25 μM and 15 μM of **1** and **2**, respectively. All the doses were given below the calculated IC_{50} and the cells are incubated for 24 h before the DAPI nuclear staining assay. When the cells are examined under a fluorescent microscope with a DAPI filter, it is found that the control cells are hardly accompnied by any sort of condensation in comparison to the activity of the test compound (as shown in Fig. 10). All images clearly demonstrate the brightly condensed chromatin bodies and the nuclear blebbings, marked by arrows in the figure. Besides nuclear changes, the drug treated groups have also revealed a shrinking morphology, which is another important hallmark of apoptosis.

3.6. DFT and TD DFT studies

We have employed the density functional theory calculations on both the complexes (**1** and **2**) to aid our interest to correlate the structure-activity relationship of coordination compounds[76]. Four possible spin interactions between unpaired electrons of both the cobalt centers have been found in **1**. The two Co(II) nuclei can be coupled either ferromagnetically or antiferromagnetically through high-high spin or low-low spin surfaces (Table 4). We have optimized all possible interactions and our computations predicted that ferromagnetic interaction (S_T=3) on high spin is found to be the ground state while other interactions are higher in energy (Table 4). The optimized structure and its corresponding spin density plot of the ground state of **1** are shown in Fig 11 (a) and rest of the possible interactions are shown in Fig 12. The presence of three unpaired electrons on each metal centre of **1** has been confirmed by the spin density values (ρ=2.662 on Co1 and ρ=2.698 on Co2) (Fig 11 (a)). Similarly, we

have also optimized **2**, which has two possible spin interactions i.e. ferromagnetic (S_T=1) or antiferromagnetic (S_T=0). We have also optimized both of these and our calculations show that ferromagnetic interaction is computed to be the ground state which is also observed in earlier studies.[77,78] The optimized structure and its corresponding spin density plot are shown in Fig 11b (for ferromagnetic) and Fig 13 (for antiferromagnetic). The spin density value (ρ=0.557) on both the Cu is same confirming the presence of one unpaired electron on each copper centre (Fig 11b). The X-ray data favor the authentication of our computed structural parameters.

The Mulliken frontier molecular orbital (FMO) composition in the ground state (S_T=3) of the **1** shows that HOMO has 22% and 44% charge contributions on the Co1 and Co2 centers, respectively and a sum of 6% on both the Schiff bases (L1 and L2) while 25% on H_2O (1) and 3% on H_2O (2) (Table 5). Next, in (H-1) and (H-2) orbitals both the metal centers have similar charge contributions; 2% on each metal atom. Whereas L1 shows 24% in (H-1) & 71% in (H-2) orbital and L2 bearing 72% in (H-1) & 24% in (H-2) orbital. Both the water molecules have no charge contribution (0%) in (H-1) orbital while H_2O (1) has 1% of charge contribution in (H-2). In (H-3) orbital, Co1 has 9% and Co2 has 68% of charge contribution and L1 & L2 have a sum of 8% of charge contribution (4% on each) whereas both the water molecules have 3% (H_2O (1)) and 12% (H_2O (2)).

Next, in (H-4) orbital Co1 has 1%, Co2 has 78%, L1 & L2 have 20% (10% on each) and H_2O (1) has 1% while H_2O (2) has no charge contribution (Table 5). In the LUMO, most of the charge is accumulated on both the L1 (69%) and L2 (28%) ligands while Co2 and both H_2O show no charge contributions. In (L+1) orbital, mostly charge is concentrate on both L1 (27%) and L2 (68%) ligands whereas Co1 has 4% and Co2 has 1% of charge contribution. Next, in (L+2) orbital, charge contribution on Co1 has increased quite high (28%) compared to (L+1) orbital. In (L+2) orbital there is no charge contribution on Co2, H_2O (1) and H_2O (2) while L1 shows 39% and L2 shows 33% charge contribution. In (L+3) orbital, Co1 shows 19%, Co2 &

H_2O (2) shows 1% on each and both L1 and L2 show 36% and 43% charge contribution, respectively. Next, in (L+4) orbital a noticeable amount of total charge (89%) is accumulated on L1, whereas L2 has 9%, Co1 and Co2 have 1% on each while both the water ligands have no charge contribution. **1** shows more charge contribution between molecular orbitals as compared to **2**. More charge contributions in metal orbitals are responsible for the enhanced catecholase activity of the complex **1**[74].

Furthermore, the metal charge contributions of the ground state (S_T=1) of **2** shows that HOMO has 2% charge contribution from each of the metal atoms and overall 4% on both metal centers while 48% from each of the ligands (L1 and L2), and overall 96% on both the ligands. In (H-1) orbital, 8% charge is present on metals (4% on each) while 92% charge is present on ligands (46% on each). In next (H-2) orbital, it is decreased with one unit (3%) on each metal center and increased one unit on each ligand with 47%. In (H-3) orbital, charge on metals increases with two units (5%) on each metal atom with total 10% on both and decreases by two units on each ligands (L1 & L2) with 45% with total 90%. Next, in (H-4) orbital, charge accumulation also increases on metal by three units (8%), aggregated with 16% on both the metals while on ligands aggregated charge accumulation is 84%. LUMO and (L+1) show same charge contribution, 1% from each metal center and overall 2% on both metals and 49% from each ligand and overall 98% on both ligands (Table 5). In (L+2) orbital, the charge contribution results are similar to HOMO *i.e.* 4% on both the metal centers (2% on each metal) and 96% on both the ligands. Next, in (L+3) orbital, the charge is totally accumulated on the ligands whereas there is no charge availability on both metals. While in next orbital (L+4) remarkable charge is concentrated with 84% (42% each) on metals and 16% on both the ligands. Low charge contribution in molecular orbitals of the complex demonstrates its negligible catecholase activity. Our computed charge distributions unfold more catecholase activity of **1** than **2**.

TD–DFT calculations have also been performed on the ground state to understand and explore the absorption spectra of **1**. Five peaks at 319, 348, 415, 571 and 812 nm have been observed (shown in Fig 14). The first peak observed at 319 nm pertaining to the metal to ligand charge transfer (MLCT) transition. The peaks at 348 and 415 nm also pertaining to the MLCT transition. The next two peaks at 571 and 812 nm indicate the *d–d* transition such as α–($Co1_{dxz}$) $\rightarrow\alpha$–($Co1_{dyz}$) and α–($Co2_{dxz}$) $\rightarrow\alpha$–($Co2_{dz}^2$), respectively. TD–DFT has also been done for the computations on the ground state of **2** to understand its electronic nature. We have got four peaks at 328, 383, 425 and 519 nm (Fig 15). The first two peaks at 328 and 383 nm show same kind of charge transfer transition *i.e.* metal to ligand charge transfer transitions whereas peak at 425 nm corresponds to ligand to metal charge transfer transition. The next peak computed at 519 nm shows *d–d* charge transfer transition *i.e.* β–(Cu_{dxy}) $\rightarrow\beta$–($Cu_{dx^2-y^2}$). These transitions are also in correlation with experimental observations.

4. Conclusion

We have designed two dinuclear (Co^{II}(**1**) and Cu^{II}(**2**)) complexes derived from Schiff base ligands to explore their coordination chemistry for biological activities. The bonding characteristics of the ligands, and distorted octahedral and square pyramidal geometry around Co^{II} and Cu^{II} centres, respectively have been confirmed by the characterization data including X-ray studies. The moderate ferromagnetic exchange between the metal centres in molecules has been ascertained by variable temperature magnetic measurements. Theoretical calculations (DFT) also support these magnetic interactions. **1** exhibits potential activity towards the oxidation of the 3,5-DTBC to 3,5-DTBQ and could be employed as model metalloenzyme (catechol oxidase). This activity has been authenticated by DFT and is attributed to the higher charge contribution on metal in case of **1** as compared to **2**. Moreover, the present complexes

(**1** and **2**) screened for HeLa and A549 cells lines have been proven to show better anticancer activity than cisplatin with $IC_{50} \approx 7.0$ at 48 h. The fluorescence microscopy reveals the apoptosis with blebbing and striking morphology as has been observed for HeLa. Thus, the results show that the present complexes seem to be promising model metalloenzymes as well as anti cancer angents and the activity can be further tuned by structural modifications. This work provides an insight to the designing and development of new dinuclear Schiff base complexes for desired biological activities.

References

1. M. B. Robin, P. Day, *Adv. Inorg. Chem. Radiochem.*, 1967, **10**, 247.

2. (a) G. C. Allen, N. S. Hush, *Prog. Inorg. Chem.*, 1967, **8**, 357; (b) N. S. Hush, *Prog. Inorg. Chem.*, 1967, **8,** 391.

3. G. Blondin, J.-J. Girerd, *Chem. Rev.*, 1990,**90**, 1359.

4. (a) W. Kaim, G. K. Lahiri, *Angew. Chem., Int. Ed.*, 2007**46**, 1778; (b) K. D. Demadis, C. M. Hartshorn, T. J. Meyer, *Chem. Rev.*, 2001, **101**, 2655; (c) W. Kaim, A. Klein, M. Glöckle, *Acc. Chem. Res.*,2000, **33**, 755; (d) D. M. D'Alessandro, F. R. Keene, *Chem. Rev.*, 2006,**106**, 2270; (e) D. M. D'Alessandro, F. R. Keene, *Chem. Soc. Rev.*,2006, **35**, 424; (f) B. S. Brunschwig, C. Creutz, N. Sutin, *Chem. Soc. Rev.*, 2002, **31**, 168.

5. N. Raman, S. Ravichandran, C. Thangaraja, *J. Chem. Sci.*, 2004, **116**, 215.

6. D. Gatteschi, R. Sessoli, *Angew. Chem., Int. Ed.*, 2003,**42**, 268;

7. A.M. Ako, V. Mereacre, Y.H. Lan, W. Wernsdorfer, R. Clérac, C.E. Anson, A.K. Powell, *Inorg. Chem.*, 2010,**49**, 1.

8. T. Taguchi, W. Wernsdorfer, K.A. Abboud, G. Christou, *Inorg. Chem.*, 2010,**49**, 199.

9. M.T. Gamer, Y.H. Lan, P.W. Roesky, A.K. Powell, R. Clérac, *Inorg. Chem.*, 2008, **47**, 6581.

10. P. Alborés, E. Rentschler, *Angew. Chem., Int. Ed.*, 2009,**48**,9366.

11. S.H. Zhang, M.F. Tang, C.M. Ge, *Z. Anorg. Allg. Chem.*,2009, **635**, 1442.

12. L.F. Ma, L.Y. Wang, X.K. Huo, Y.Y. Wang, Y.T. Fan, J.G. Wang, S.H. Chen, *Cryst. Growth Des.*, 2008, **8**, 620.

13. S.H. Zhang, Y.L. Zhou, X.J. Sun, L.Q. Wei, M.H. Zeng, H. Liang, *J. Solid State Chem.*, 2009, **182**, 2991.

14. S.H. Zhang, Y. Song, H. Liang, M.H. Zeng, *CrystEngComm.*, 2009,**11**, 865.

15. Q. Liang, R. Huang, X. Chen, Z. Li, X. Zhang, B. Sun, *Inorg. Chem. Commun.*, 2010,**13**, 1134.

16. S.S. Tandon, S.D. Bunge, R. Rakosi, Z. Xu, L.K. Thompson, *Dalton Trans.*, 2009, 6536.

17. H.L.C. Feltham, R. Clérac, S. Brooker, *Dalton Trans.*, 2009, 2965.

18. M. Nihei, N. Hoshino, T. Ito, H. Oshio, *Polyhedron*, 2003,**22**, 2359.

19. S. Hazra, R. Koner, P. Lemoine, E.C. Sañudo, S. Mohanta, *Eur. J. Inorg. Chem.*, 2009, 3458

20. (a) S. Zhang, W. Chen, B. Hu, Y. Chen, L. Zheng, Y. Li, W. Li, *J. Organomet. Chem.*,2012, **65**, 4147;(b) T. Shiga, H. Oshio, *Polyhedron*, 2011,**30**, 3238.

21. M. Emami, N. Noshiranzadeh, R. Bikas, A. Gutierrez and A. kozakiewicz *Polyhedron.*, 2017,**122**, 137.

22. (a) A.-M.-C. Dumitriu, M. Cazacu, A. Bargan, S. Shova, C. Turta, *Polyhedron*, 2013,**50**, 255; (b) A.K. Ghosh, A. Bauzá, V. Bertolasi, A. Frontera, D. Ray, *Polyhedron*, 2013,**53**, 32.

23. (a) M. Pait, E. Colacio, D. Ray, *Polyhedron*, 2015,**88**, 90; (b) P. Mondal, A. Hens, K.K. Rajak, *Polyhedron*, 2013,**54,** 228.

24. S. Majumder, S. Sarkar, S. Sasmal, E. C. Sañudo and S. Mohanta, *Inorg. Chem.*, 2011,**50**, 7540.

25. (a) S. Mukherjee, T. Weyhermüller, E. Bothe, K. Wieghardt, P. Chaudhuri, *Dalton Trans.*, 2004, 3842;(b) A. Majumder, S. Goswami, S. R. Batten, M. S. E. Fallah, J. Ribas, S. Mitra, *Inorg. Chim. Acta.*, 2006, **359**, 2375; (c) G. Blay, I. Fernández, J. R. Pedro, R. Ruiz-García, T. Temporal-Sánchez, E. Pardo, F. Lloret, M. C. Muñoz, *J. Mol. Catal. A: Chem.*, 2006, **250**, 20; (d) M. U. Triller, D. Pursche, W.-Y. Hsieh, V. L. Pecoraro, A. Rompel, B. Krebs, *Inorg. Chem.*,2003, **42**, 6274.

26. (a) I. Cs. Szigyártó, L. I. Simándi, L. Párkányi, L. Korecz, G. Schlosser, *Inorg. Chem.*, 2006,**45**, 7480; (b) J. Kaizer, R. Csonka, G. Baráth, G. Speier, *Transition Met. Chem.*,2007, **32**, 1047;(c) T. L. Simándi, L. I. Simándi, *J. Chem. Soc., Dalton Trans.*, 1999, 4529.

27. (a) T. L. Simándi, L. I. Simándi, *React. Kinet. Catal. Lett.*, 1998, **65**, 301; (b) L. I. Simándi, T. L. Simándi, *J. Chem. Soc., Dalton Trans.*,1998 3275; (c) C. R. K. Rao, P. S. Zacharias, *Polyhedron*, 1997,**16**, 1201.

28. S. Banerjee, M. Nandy, S. Sen, S. Mandal, G. M. Rosair, A. M. Z. Slawin, C. J. G. García, J. M. Clemente-Juan,E. Zangrando, N. Guidolin, S. Mitra, *Dalton Trans.*, 2011, 1652.

29. T. S. M. Abedin, L. K. Thompson, D. O. Miller,*Chem. Commun.*, 2005, 5512; (b) I. C. Lazzarini, L. Carrella, E. Rentschler, P. Alborés, *Polyhedron*, 2012, **31**, 779.

30. L. Dai, J. Liu, Z. Luo, M. Li, K. Cai, *J. Mater. Chem. B*, 2016,**4**, 6758.

31. (a) N. J. Wheat, S. Walker, G. E. Craig, R. Oun, *Dalton Trans.*,2010, **39**, 8113; (b) M. Vitali, C. I. Ripamonti, F. Roila, C. Proto, D. Signorelli,M. Imbimbo, G. Corrao, A. Brissa, G. Rosaria, F. de Braud,M. C. Garassino, G. Lo Russo, *Crit. Rev. Oncol.Hematol.*, 2017, **118**, 7.

32. (a) C. Holohan, S. Van Schaeybroeck, D. B. Longley, P. G. Johnston, *Nat. Rev. Cancer*, 2013, **13**, 714; (b) J. Chien, R. Kuang, C. Landen, V. Shridhar, *Front Oncol*.,2013, **3**, 1.

33. I. Romero-Canel´on, P. J. Sadler, *Inorg. Chem.*, 2013, **52**,12276.

34. (a) C. Santini, M. Pellei, V. Gandin, M. Porchia, F. Tisato, C. Marzano, *Chem. Rev.*, 2014, **114**, 815; (b) I. Iakovidis, I. Delimaris, S. M. Piperakis, *Mol. Biol. Int.*,2011, **2011**, 1.

35. A. Biswas, L. K. Das, M. G. B. Drew, G. Aromí, P. Gamez, A. Ghosh,*Inorg. Chem.*, 2012,**51**, 7993

36. S. Majumder, S. Mondal, P. Lemoine, S. Mohanta,*Dalton Trans.,* 2013, **42**, 4561.

37. L. Mandal, S. Sasmal, H.A.Sparkes, J. A.K.Howard, S. Mohanta, *Inorg. Chim. Acta.*,2014, **412**, 3845.

38. R. Modak, Y. Sikdar, S. Mandal, S. Goswami, *Inorg.Chem. Commun.*, 2013, **37**, 193.

39. K. G. Alley, G. Poneti, J. B. Aitken, R. K. Hocking,B.Moubaraki, K. S. Murray, B. F. Abrahams, H. H. Harris,L. Sorace, C. Boskovic, *Inorg. Chem.*, 2012, **51**, 3944.

40. Y. Mulyana, G. Poneti, B. Moubaraki, K. S. Murray,B. F. Abrahams, L. Sorace, C. Boskovic, *Dalton Trans.*, 2010,**39**,4757.

41. C. Carbonera, A. Dei, J.-F. Letard, C. Sangregorio, L. Sorace, *Angew. Chem., Int. Ed.*,2004, **43**, 3136.

42. A. Caneschi, A. Dei, *Angew. Chem., Int. Ed.*, 1998, **37,** 3005.

43. D. M. Adams, A. Dei, A. L. Rheingold, D. N. Hendrickson, *J. Am. Chem. Soc.*, 1993,**115**, 8221.

44. S. K. Dey, A. Mukherjee,*New J. Chem.*, 2014,**38**, 4985.

45. J. A. Ibers, W. C. Hamilton, International Tables for X-ray Crystallography, Kynoch Press, Birmingham, England, 1974, vol. IV.

46. SMART & SAINT Software Reference manuals, Version 6.45, Bruker Analytical X-ray Systems, Inc., Madison, WI, 2003.

47. G. M. Sheldrick, SADABS, software for empirical absorption correction, Ver. 2.05, University of Göttingen, Göttingen, Germany, 2002.

48. XPREP, version 5.1, Siemens Industrial Automation Inc.,Madison, WI, 1995.

49. G. M. Sheldrick, SHELXL97, Program for Crystal Structure Refinement, University of Göttingen, Göttingen, Germany, 2008.

50. G. M. Sheldrick, *Acta Cryst. C.*, 2015,**71**, 3.

51. S. Mukhopadhyay, P. K. Panda, B. Behera, C. K. Das, M. K. Hassan, D. N. Das, N. Sinha, A. Bissoyi, K. Pramanik,T. K. Maiti, S. K. Bhutia, *Food Chem. Toxicol.*, 2014, **64**, 369.

52. S. Mukhopadhyay, P. K. Panda, D. N. Das, N. Sinha, B. Behera, T. K. Maiti, S. K. Bhutia, *Acta Pharmacol.Sin.*, 2014, **35**, 814.

53. M. J. Frisch, G. W. Trucks, H. B. Schlegel, G. E. Scuseria, M. A. Robb, J. R. Cheeseman, G. Scalmani, V. Barone, B. Mennucci, G. A. Petersson, H. Nakatsuji, M. Caricato, X. Li, H. P. Hratchian, A. F. Izmaylov, J. Bloino, G. Zheng, J. L. Sonnenberg, M. Hada, M. Ehara, K. Toyota, R. Fukuda, J. Hasegawa, M. Ishida, T. Nakajima, Y. Honda, O. Kitao, H. Nakai, T. Vreven, J. A. Montgomery Jr., J. E. Peralta, F. Ogliaro, M. Bearpark, J. J. Heyd, E. Brothers, K. N. Kudin, V. N. Staroverov, R. Kobayashi, J. Normand, K. Raghavachari, A. Rendell, J. C. Burant, S. S. Iyengar, J. Tomasi, M. Cossi, N. Rega, J. M. Millam, M. Klene, J. E. Knox, J. B. Cross, V. Bakken, C. Adamo, J. Jaramillo, R. Gomperts, R. E. Stratmann, O. Yazyev, A. J. Austin, R. Cammi, C. Pomelli, J. W. Ochterski, R. L. Martin, K. Morokuma, V. G. Zakrzewski, G. A. Voth, P. Salvador, J. J. Dannenberg, S. Dapprich, A. D. Daniels, Ö. Farkas, J. B. Foresman, J. V. Ortiz, J. Cioslowski and D. J. Fox, GAUSSIAN 09 (*Revision 2*), Gaussian, Inc., Wallingford, CT, 2009.

54. A. D. Becke, *J. Chem. Phys.*, 1993, **98**, 5648.

55. C. Lee, W. Yang, R. G. Parr, *Phys. Rev. B: Condens. Matter Mater. Phys.*, 1988, **37**, 785.

56. S. Grimme, J. Antony, S. Ehrlich, H. Krieg, *J. Chem. Phys.,*2010, **132**, 154104 (1–18).

57. A. Ansari, A. Kaushik, G. Rajaraman, *J. Am. Chem. Soc.*, 2013, **135**, 4235.

58. T. H. Jr. Dunning, P. J. Hay, *In Modern Theoretical Chemistry*; H. F. Schaefer, III Ed.; Plenum: New York, 1976,**Vol. 3**, pg–1.

59. P. J. Hay, W. R. Wadt, *J. Chem. Phys.,*1985, **82**, 270.

60. W. R. Wadt, P. J. Hay, *J. Chem. Phys.,*1985,**82**, 284.

61. P. J. Hay, W. R. Wadt, *J. Chem. Phys.,* 1985,**82**, 299.

62. R. Ditchfield, W. J. Hehre, J. A. Pople, *J. Chem. Phys.,*1971, **54**, 724.

63. B. Mennucci, *Comput. Mol. Sci*., 2012, **2**, 386.

64. A. Schaefer, H. Horn, R. Ahlrichs, *J. Chem. Phys.*, 1992, **97**, 2571.

65. C. Schaefer, C. Huber, R. Ahlrichs, *J. Chem. Phys.,*1994, **100**, 5829.

66. F. Neese, the ORCA program system, *version 4.0*, University of Bonn, Bonn, Germany, 2009.

67. L. Skripnikov, *Chemmisian*, a computer program to analyze and visualize quantum-chemical calculations. <*www.chemissian.com*>

68. K. Nakamoto, Infrared and Raman spectra of Inorganic and Coordination Compound, John Wiley and Sons, New York, 3rd edn, 1996.

69. A. B. P. Lever, Inorganic Electronic Spectroscopy, Elsevier, Amsterdam, 1984.

70. (a) R. Pattacini, P. Teo, J. Zhang, Y. Lan, A. K. Powell, J. Nehrkorn, O. Waldmann, T. S. Andy Hor, P. Braunstein, *Dalton Trans.*, 2011, **40**, 10526; (b) F. Klöwer, Y. Lan, J. Nehrkorn, O. Waldmann, C. E. Anson, A. K. Powell, *Chem.–Eur. J.*, 2009, **15**, 7413; (c) O. Waldmann, M. Ruben, U. Ziener, P. Müller, J. M. Lehn, *Inorg. Chem.*, 2006, **45**, 6535.

71. M. E. Lines, J. Chem. Phys., 1971, **55**, 2977.

72. O. Kahn, Molecular Magnetism, VCH, New York, Weinheim and Cambridge, 1993.

73. M. N. Ahamad, F. Sama, M. N.Akhtar, Y. –C. Chen, M. -L. Tong, M. Ahmad, M. Shahid, S. Hussain, K. Khan. *New J. Chem.* 2017,**41,** 14057.

74. F. Sama, A. K.Dhara, M. N. Akhtar, Y. -C. Chen, M.-L. Tong, I. A. Ansari, M. Raizada, M. Ahmad, M. Shahid, Z. A. Siddiqi, *Dalton Trans.*, 2017, **46**, 9801.

75. M. Ahmed, K. Jamil, *Biol. Med.*, 2011,**3**, 60.

76. (a) M. N. Ahamad, M. Shahid, A. Ansari, M. Kumar, I. M. Khan, M. Ahmad, Rahisuddin, R. Arif, *New J. Chem.,* 2019, **43**, 7511–7519. (b) M. N. Ahamad, M. Kumar, A. Ansari, Mantasha I., M. Ahmad, M. Shahid, *New J. Chem.*, 2019,**43**, 14074. (c) A. Ansari, P. Jayapal and G. Rajaraman, *Angew. Chem. Int. Ed.* 2015, **54**, 564-568. (d) A. Ansari and G. Rajaraman, *Inorg. Chem.* 2015, **54**, 11077-11082. (e) A. Ansari and G. Rajaraman, *Phys. Chem. Chem. Phys.* 2014, **16**, 14601-14613.

77. (a) E. Safaei, A. Wojtczak, E. Bill, H. Hamidi, *Polyhedron*, 2010, **29**, 2769. (b) E. Safaei, M. Rasouli, T. Weyhermuller, E. Bill, *Inorg. Chim. Acta*, 2011, **375**, 158.

78. A. Jana, S. Konar, K. Das, S. Ray, J. A. Golen, A. L. Rheingold, L. M. Carrella, E. Rentschler, T.K. Mondal, S.K. Kar, *Polyhedron*, 2012, **38**, 258.

Graphical Abstract

Two Schiff base dinuclear Co_2 and Cu_2 complexes are designed, characterized and evaluated for catecholase and anticancer activities. The magnetic and biological properties are beautifully corroborated by theoretical (DFT/TD-DFT) calculations. Insights into the structure-activity relationship would lead tune the properties for future endeavours.

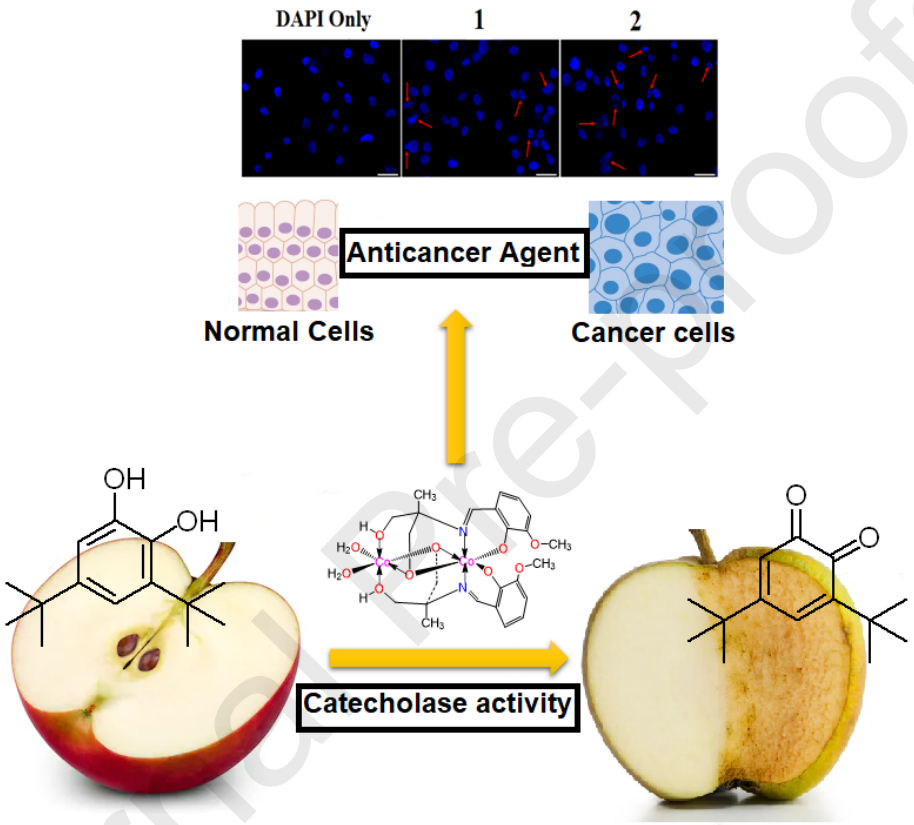

Highlights

- Two new Schiff base complexes are designed and characterised.
- The complexes exhibit potent anticancer activity toward HeLa (cervical) and A549 (lung) cancer cell lines with IC_{50} = 6-7 μM at 48 h.
- The complexes exhibit apoptosis of Hela cells by demonstrating nuclear blebbings with shrinking morphology.
- Co(II) complex (**1**) exhibited enhanced catecholase like activity (for oxidation of 3,5-di-tert-butylcatechol to corresponding quinone) with K_{cat}= 213.48 h^{-1}.
- This catecholase like activity is attributed to the greater extent of charge contribution on Co^{2+} as compared to Cu^{2+} as determined by DFT calculations.
- Experimental results are corroborated well by theoretical calculations.

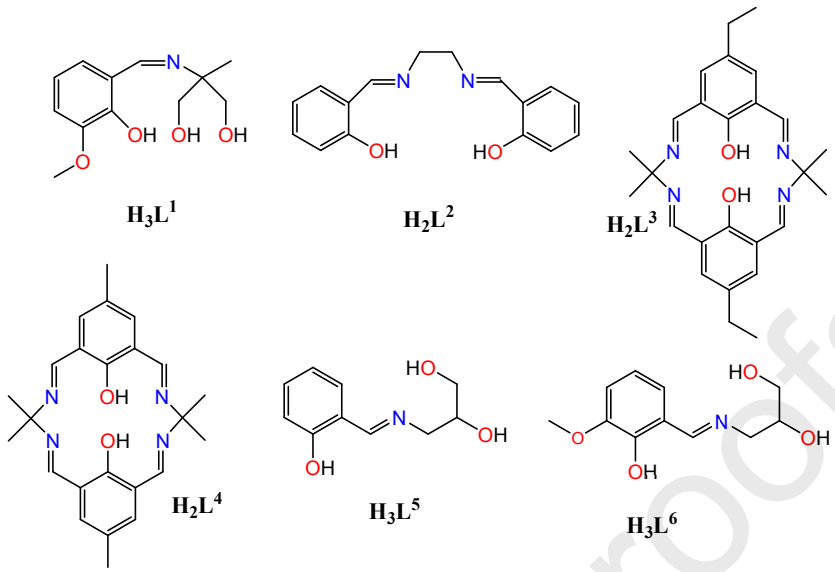

Scheme 1. Structures of some Schiff base ligands used to prepare dinuclear complexes.[36-44]

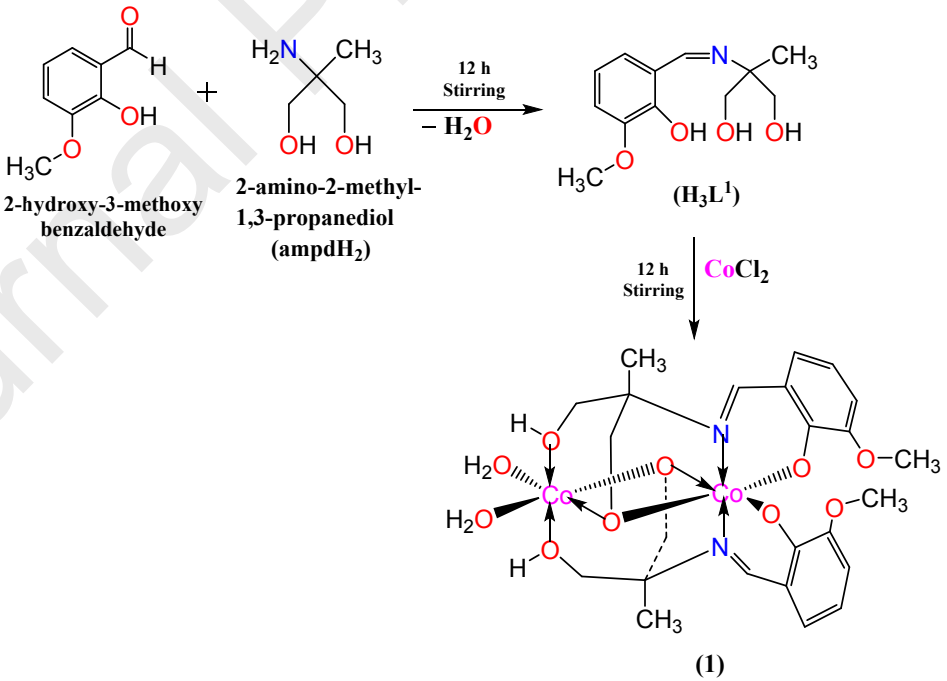

Scheme 2. Synthetic procedure for **1**.

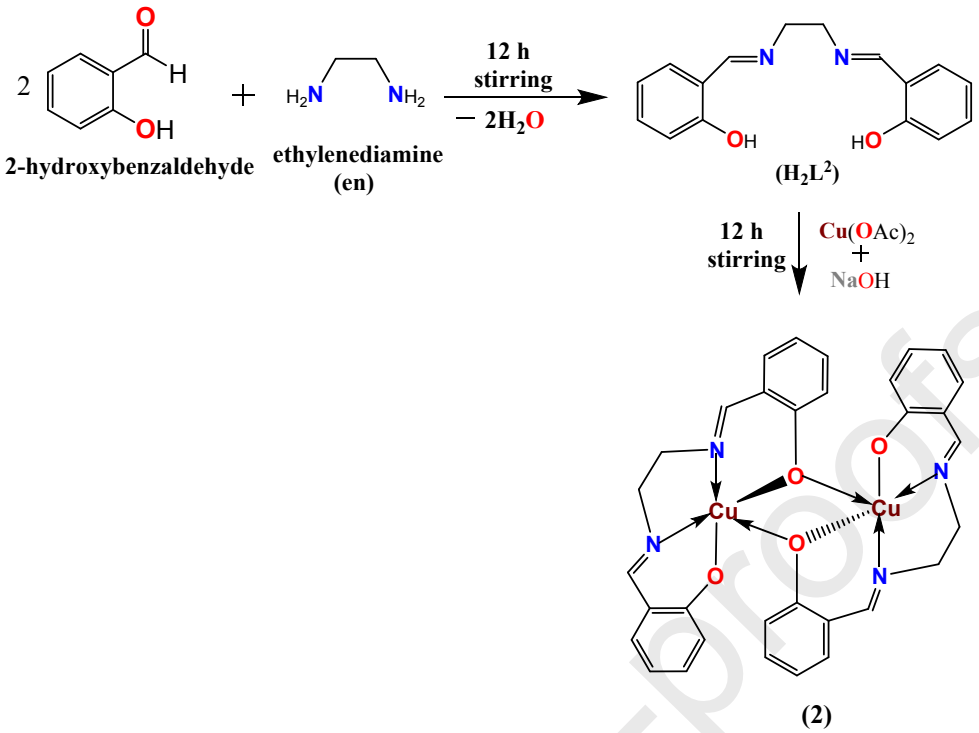

Scheme 3. Synthetic procedure for **2**.

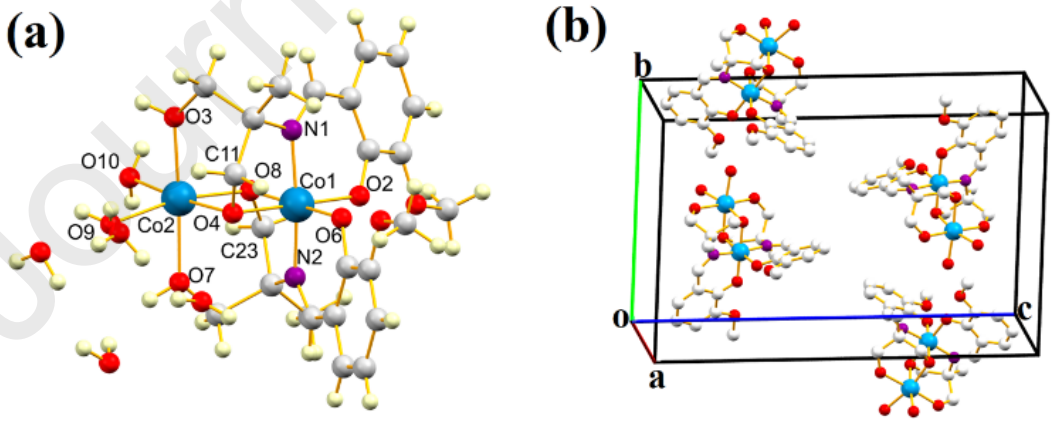

Fig. 1. (a) Perspective view of **1** (lattice species omitted for clarity). **(b)** Packing of diagram of **1**.

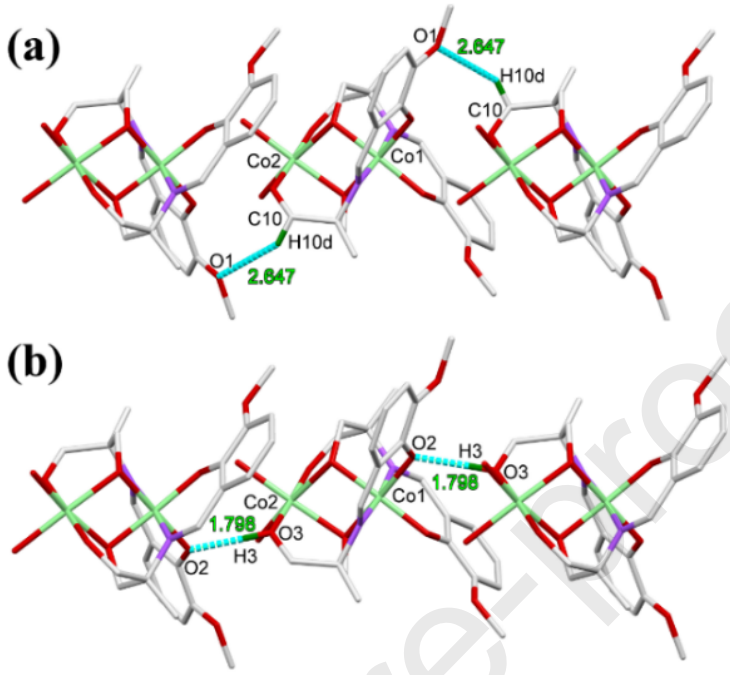

Fig. 2. (**a**) 1D chain generated as a result of C–H---O interactions. (**b**) 1D chain generated as a result of O–H---O interactions.

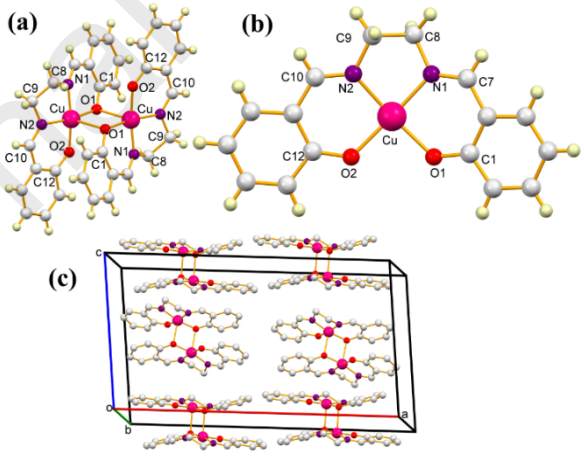

Fig. 3. (a) ORTEP view of **2**. **(b)** asymmetrical structural unit of **2**. **(c)** Packing diagram of **2**.

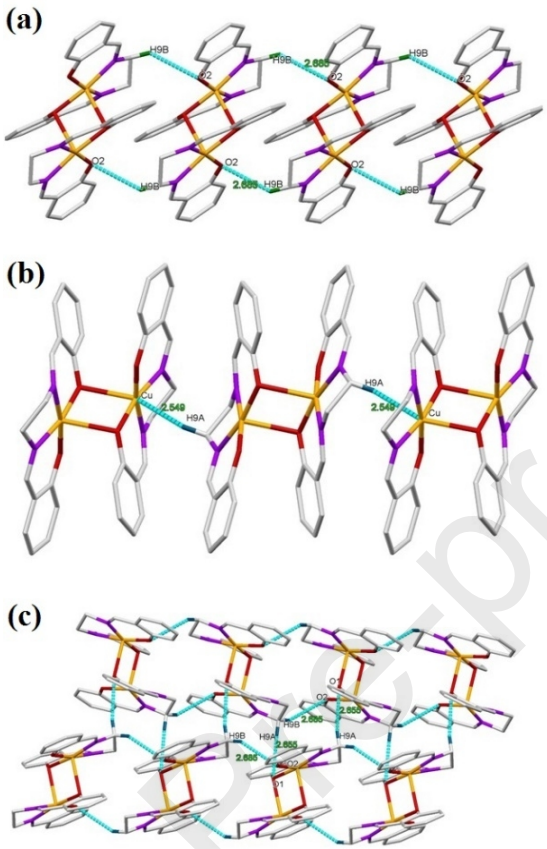

Fig. 4. (a) 1D polymer of **2** due to C–H---O interactions. **(b)**1D polymer of **2** due to C-H----M interactions.**(c)**2D sheet formed by various H-bonding interactions.

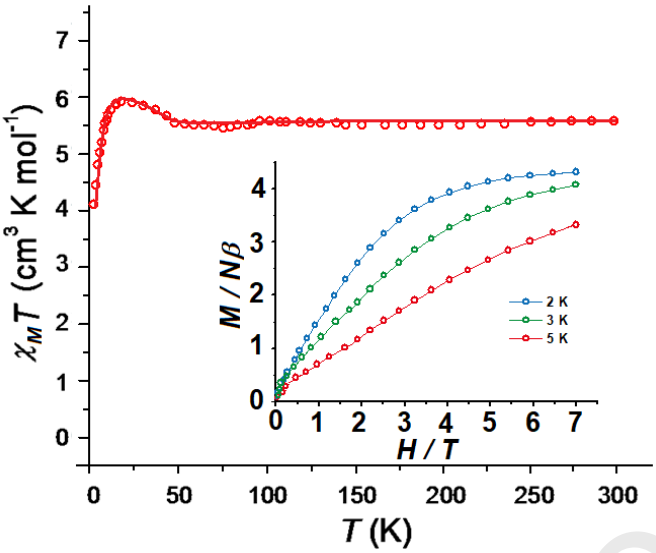

Fig.**5**. χT *vs.* T plot of magnetic susceptibility for **1**. The solid line in the main plot represents the best-fit with the L-S model to the magnetic data of **1**. Inset: Magnetization as M *vs.* H for **1**. The dots represent the measured data, while the solid lines represent the best fits using the effective model.

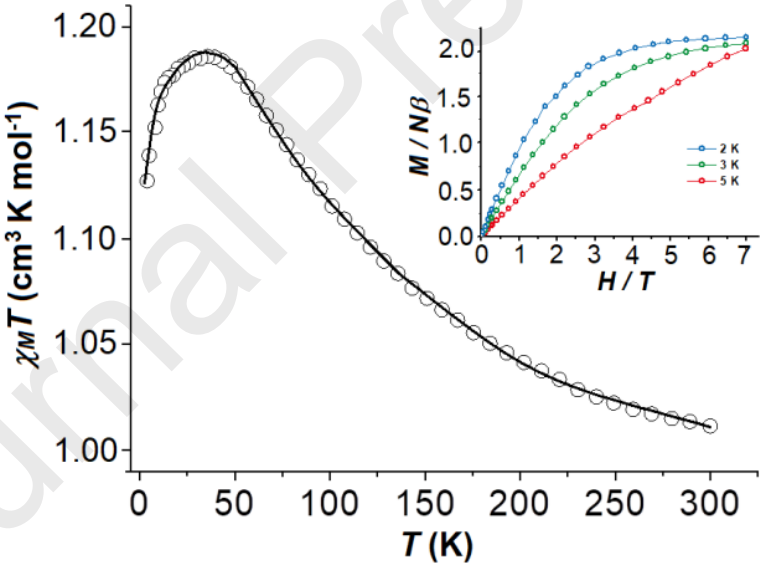

Fig.**6**. χT *vs.* T plot of magnetic susceptibility for **2**. The solid line in the main plot represents the best-fit with the L-S model to the magnetic data of **2**. Inset: Magnetization as M *vs.* B for **2**. The dots represent the measured data, while the solid lines represent the best fits using the effective model.

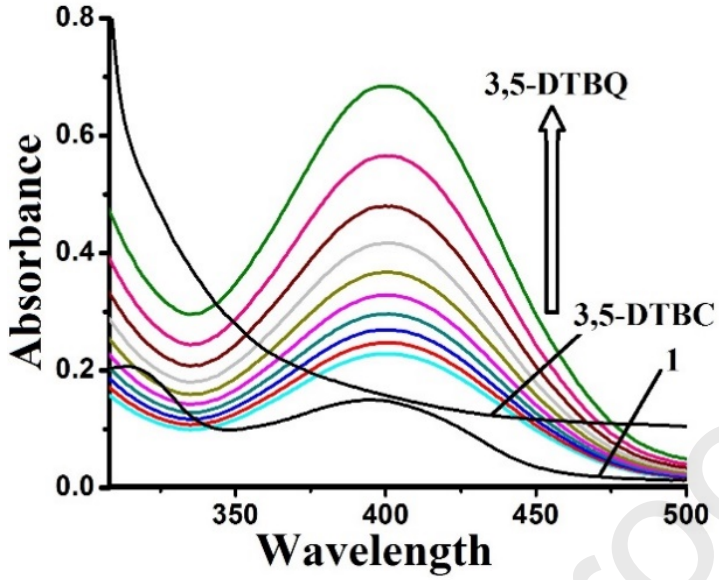

Fig. 7. UV- Visible spectrum of **1** and 3,5-DTBC and changes in UV-visible spectrum of **1** upon addition of 3,5-DTBC.

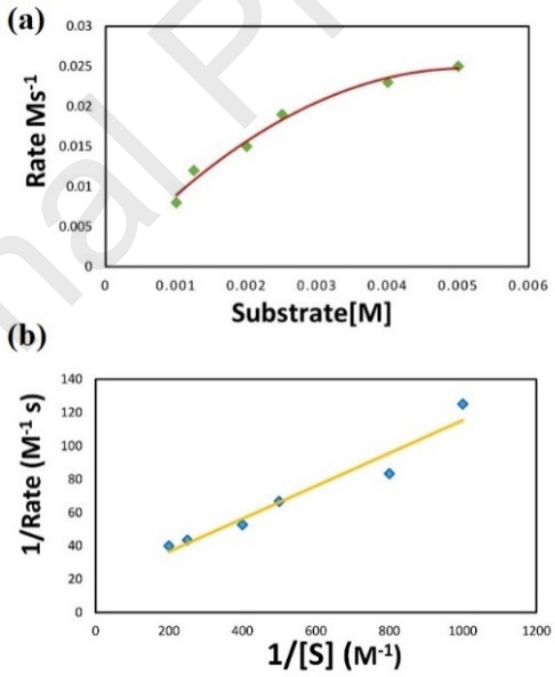

Fig. 8. (a) Initial rates versus substrate concentration for the 3,5-DTBC→3,5- DTBQ oxidation reaction catalyzed by **1** in methanol. **(b)** The Lineweaver–Burk plot (Symbols and solid lines represent the observed and simulated profiles, respectively).

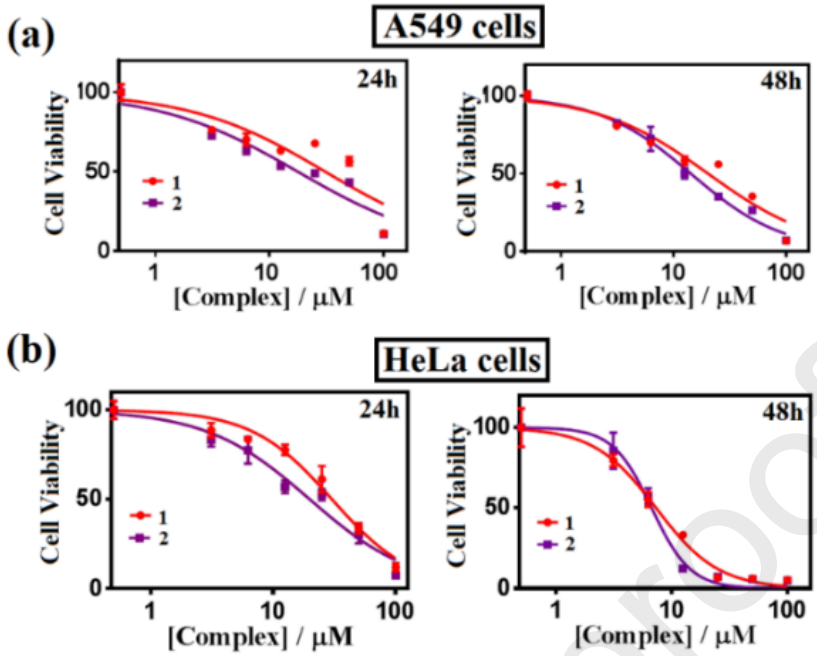

Fig. 9. Plots representing the effect of **1** and **2** on cancer cell viability and growth: A549 (a) and HeLa (b) cells upon treatment with different concentrations of the test compounds for 24 h and 48 h and then cell viability is measured by the MTT assay.

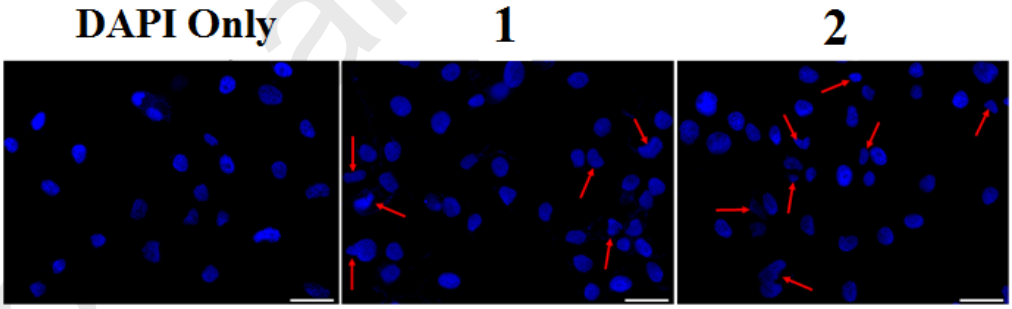

Fig. 10. Representative morphological changes observed in nuclei of HeLa cells: after treatment, HeLa cells from the control and the treated group were fixed with 3.7% formaldehyde for 15 min, permeabilized with 0.1% Triton X-100 and stained with 1 μg ml−1 DAPI for 5 min at 37 °C. The cells were then washed with PBS and examined by fluorescence microscopy (Olympus IX 71) (200×).

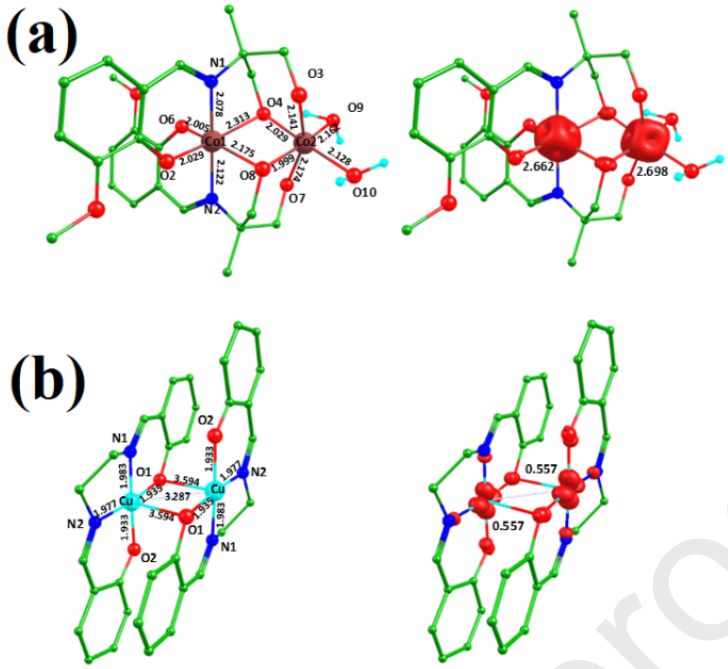

Fig. 11. B3LYP-D2 optimized structures and their spin density plots of the ground state of (a) **1** and (b) **2**.

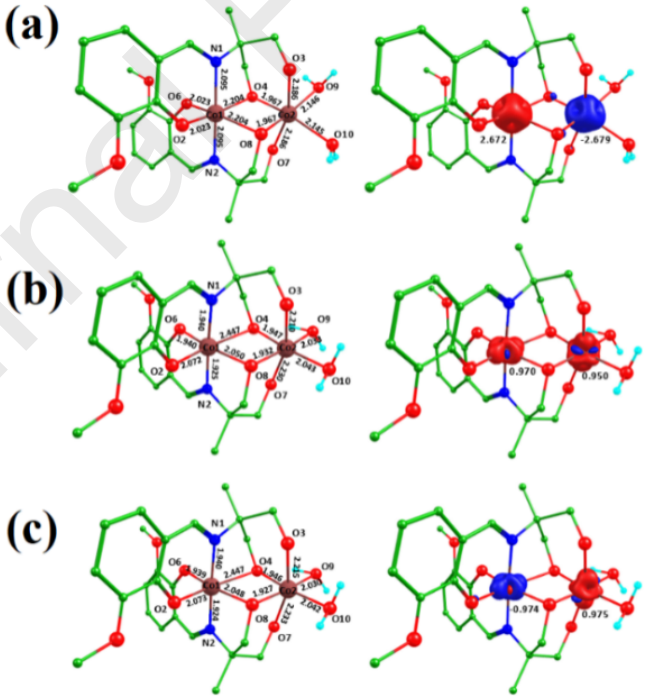

Fig. 12. B3LYP–D2 optimized structures of (a) antiferromagnetic (S_T=0), (b) ferromagnetic (S_T=1) and (c) antiferromagnetic (S_T=0) of the **1** and their corresponding spin density plots.

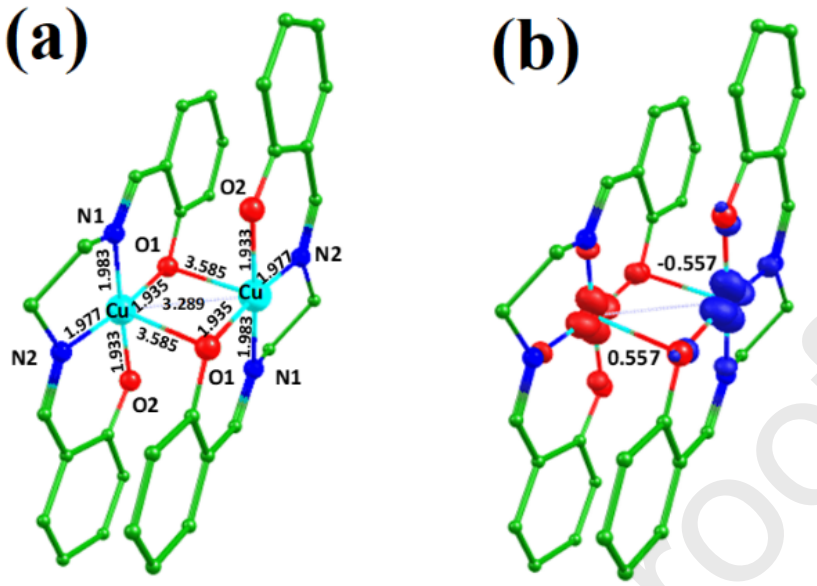

Fig. 13. B3LYP–D2 optimized structure of antiferromagnetic interaction (S_T=0) of **2** and its corresponding spin density plot.

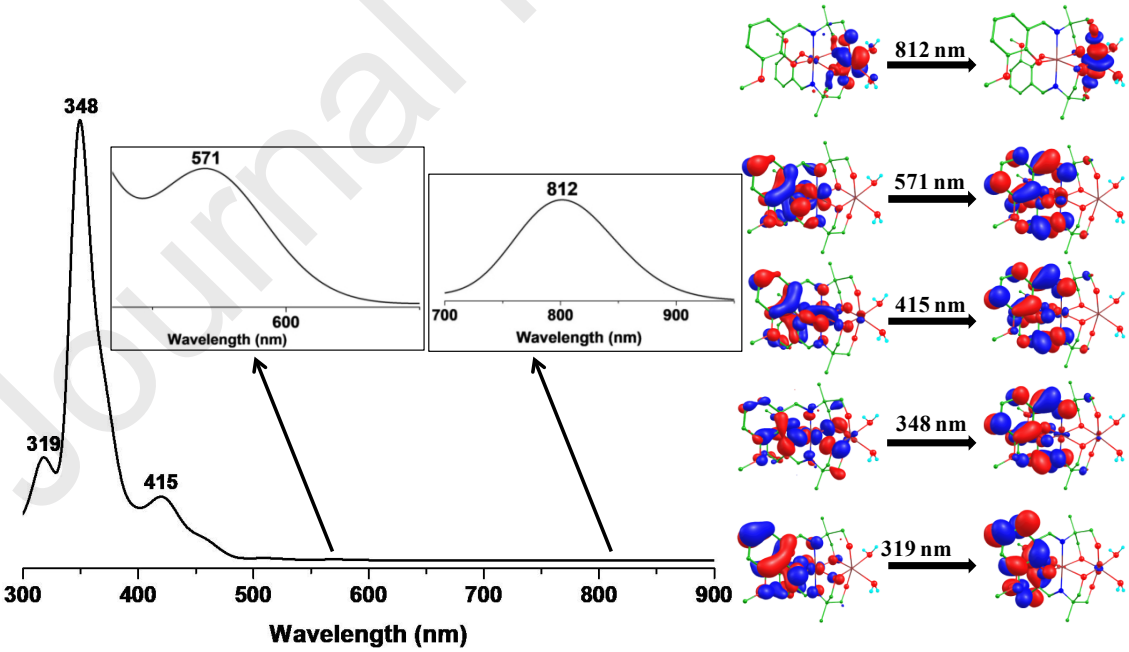

Fig. 14. B3LYP TD–DFT simulated electronic absorption spectrum of the ground state (ST=3) of the **1** and its corresponding orbitals involved in the transitions.

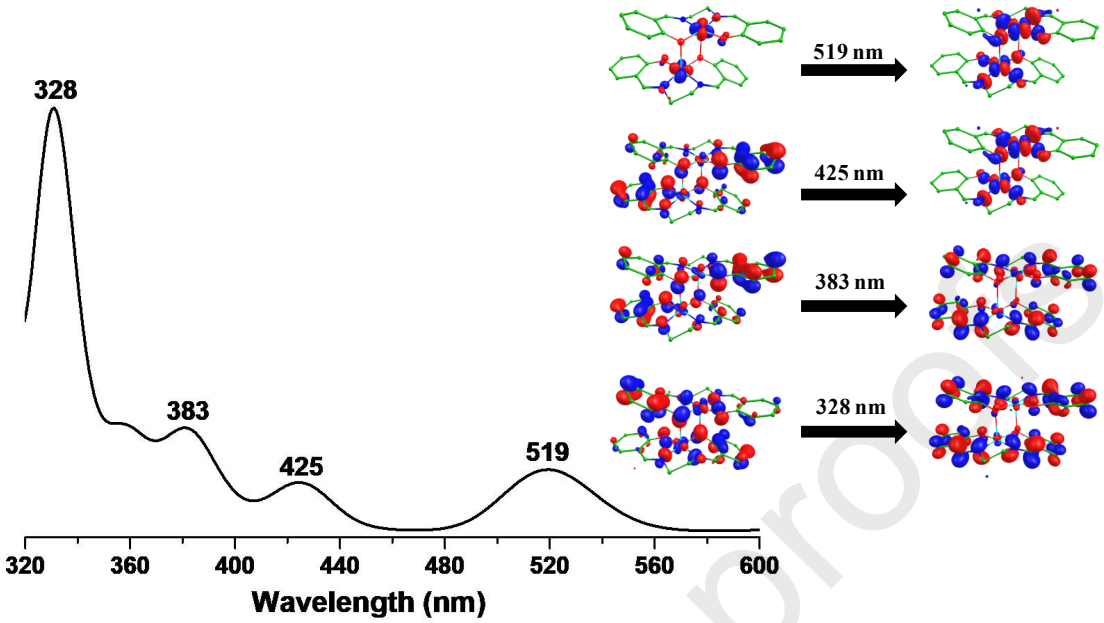

Fig.15. B3LYP TD–DFT simulated electronic absorption spectra of the ground state (S_T=1) of **2** and its corresponding orbitals involved in the transitions.

Table 1. Crystal data with refinement parameters for **1** and **2**.

	1	**2**
Molecular formula	$C_{24}H_{42}Co_2N_2O_{14}$	$C_{32}H_{28}Cu_2N_4O_4$
$\rho_{calc.}$(g cm^{-3})	1.4716	1.654
μ, mm^{-1}	1.116	1.654
Formula weight	700.48	659.66
T , K	273.15	293(2)
Crystal system	monoclinic	monoclinic
Space group	P $2_1/c$	*C2/c*
a, Å	9.7329(7)	26.594(2)
B, Å	14.3327(11)	6.9048(6)
C, Å	22.7407(16)	14.5534(11)
A, °	90	90
B, °	94.779(2)	97.573(4)
Γ,°	90	90
h	-12≤h≤12	-31≤h≤31
k	-19≤k≤19	-8≤k≤8
l	-30≤l≤30	-17≤l≤17
V, Å^3	3161.3(4)	2649.1(4)
Z	8	4
Wavelength, Å	0.71073	0.71073
Radiation type	MoKα	MoKα
Θ min, °	2.10	3.035
Θ max, °	28.29	24.990
Independent Refl.	7822	2324
Reflections collected	5412	2127
wR2 (all data)	0.2413	0.0581
wR2	0.1986	0.0558
R1 (all data)	0.0294	0.0294
R1	0.0723	0.0254

Complex	IC_{50} A549 (μM)		IC_{50} HeLa (μM)	
	24 hr	48 hr	24 hr	48 hr
1	30.88	20.29	30.20	7.339
2	17.74	14.25	19.89	6.722
cisplatin	21.3	40	10.5	16

Table 2. Summary of kinetic parameters for oxidation of DTBC of different dinuclear Co complexes with ligands given in Scheme 1 and the present complex (**1**).

Complexes	K_{cat}[h^{-1}]	K_M[M]	V_{max}[Mmin^{-1}]	Ref.
$[Co_2L^3(N_3)_3]$	482.16	0.003011	2.009×10^{-4}	36
$[Co_2L^3(N_3)_3]$	45.38	0.001576	1.891×10^{-5}	36
$[Co_2L^4(N_3)_3]$	114.24	0.001179	4.76×10^{-5}	37
$[Co_2(HL^5)_2(H_2O)(CH_3CH_2OH)]^+$	21 408	0.008815	3.56×10^{-2}	38
$[Co^{III}Co^{II}_2(H_2L^6)_2(L^4)Cl_2]$	24353	0.008972	4.05×10^{-2}	38
1	213.48	0.00584	5.93×10^{-2}	This work

Table 3. IC_{50} values of **1** and **2** against cancer cell lines.

Table 4. Various possible spin state configurations of **1** and **2**.

Spin States	Spin Interactions	Metal1	Metal2	Relative Energy (kJ/mol)
		1		
S_T=3	Ferromagnetic	↑↓↑↓↑↑↑	↑↓↑↓↑↑↑	0
S_T=0	Antiferromagnetic	↑↓↑↓↑↑↑	↑↓↑↓↓↓↓	393.5
S_T=1	Ferromagnetic	↑↓↑↓↑↓↑	↑↓↑↓↑↓↑	100.2
S_T=0	Antiferromagnetic	↑↓↑↓↑↓↑	↑↓↑↓↑↓↓	337.5
		2		
S_T=1	Ferromagnetic	↑↓↑↓↑↓↑↓↑	↑↓↑↓↑↓↑↓↑	0
S_T=0	Antiferromagnetic	↑↓↑↓↑↓↑↓↑	↑↓↑↓↑↓↑↓↓	151.9

Table 5. The Mulliken frontier molecular orbital (FMO) compositions in ground state of **1** and **2**.

		% Contributions					
		1					
Orbital	**Energy (in eV)**	**Metal1**	**Metal2**	**L1**	**L2**	**H_2O (1)**	**H_2O (2)**
H-4	-5.515	1	78	10	10	1	0
H-3	-5.135	9	68	4	4	3	12
H-2	-4.867	2	2	71	24	1	0
H-1	-4.293	2	2	24	72	0	0
H	-4.215	22	44	3	3	25	3
L	-0.967	3	0	69	28	0	0
L+1	-0.624	4	1	27	68	0	0
L+2	-0.574	28	0	39	33	0	0
L+3	-0.094	19	1	36	43	0	1
L+4	0.435	1	1	89	9	0	0
		2					

H-4	-5.727	8	8	42	42	-
H-3	-5.442	5	5	45	45	-
H-2	-5.209	3	3	47	47	-
H-1	-5.191	4	4	46	46	-
H	-5.058	2	2	48	48	-
L	-1.397	1	1	49	49	-
L+1	-1.319	1	1	49	49	-
L+2	-1.176	2	2	48	48	-
L+3	-1.144	0	0	50	50	-
L+4	0.532	42	42	8	8	-

There are no conflicts to declare by authors.